Review of the Ewald construction (Ch6)

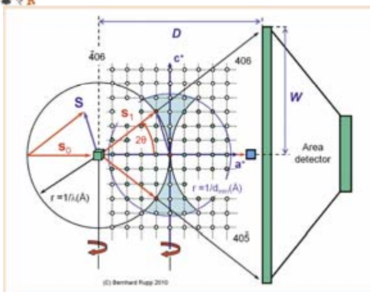

Figure 8-22 **Ewald sphere and diffraction limits.** The figure shows the Ewald sphere, centered at the crystal, its reciprocal lattice, and reciprocal lattice points which fulfill the diffraction condition (red dots). Diffraction can only be observed for reciprocal lattice points that lie inside the resolution sphere (blue circle). If a reciprocal axis is aligned with the rotation axis, a small number of reflections along the rotation axis (blue zone) are never recorded. The fraction of reflections lost in this blind region is generally low (less than 5% at 2 Å with 1.54 Å Cu radiation), smaller at shorter wavelengths, and only significant if crystals diffract to high resolution (i.e. large θ-angles).[47]

Rotation of the crystal also rotates the reciprocal lattice – by rotation we can bring more lattice points to intersect the Eqald sphere and diffraction occurs.

Rotation images are the most common mode of macromolecular diffraction data collection

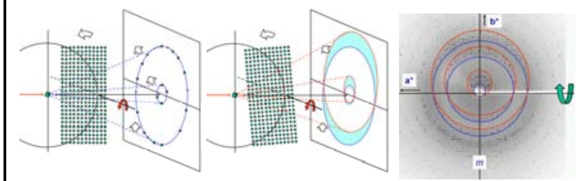

Figure 8-23 **Diffraction lunes in a rotation image.** The upper left panel shows a projection of the reciprocal lattice (RL) viewed down the rotation axis (perpendicular to the plane) at the beginning of the rotation. A few spots already lie on the Ewald sphere and with this particular RL oriented perpendicular to the incoming beam, their reflections are located on a circle. During the rotation of the crystal neighboring reciprocal lattice points (RLPs) come successively into diffraction condition (red points on Ewald sphere in lower left panel). With a dense reciprocal lattice, many reflections will fill the (cyan) area—the diffraction lune—between beginning and endpoint of the rotation (lower left panel, and also seen in the actual diffraction image in the right panel). If the RL is arbitrarily aligned relative to the rotation axis and X-ray beam, the lunes will not appear as distinct as in this drawing. Similar helpful drawings are shown in Z. Dauter's review.[48] The right panel shows an actual diffraction pattern for the same scenario, where the **a***-axis (and in the case of this orthogonal lattice also the crystal **a** axis) is aligned with the φ rotation axis. Note that from the presence of the mirror symmetry in reciprocal space along the **b*** direction we can already make an inference about the symmetry of the crystal. The mirror symmetry *m* results from combination of a 2-fold axis parallel to **b*** with the centrosymmetry of the reciprocal lattice. Therefore, the lattice symmetry contains at least a 2-fold axis parallel to **b**. We also see that the lattice spacing in both **a*** and **b*** directions is approximately equal. Together with the orthogonal axes, we thus suspect tetragonal lattice symmetry. The emphasis here is on suspect; the single image in only one orientation (corresponding to one small 1° φ-rotation) is not enough to accurately determine the lattice symmetry by visual inspection alone. The diffraction image (courtesy of Jim Pflugrath, Rigaku Americas) is in fact from a tetragonal lysozyme crystal. Note that the beam stop (white shadow) is aligned with the rotation axis: in this case blocked diffraction spots fall in the Lorentz exclusion region, and loss of reflections is minimized.

Data processing delivers an integrated, scaled, merged set of unique data

Figure 8-24 **Crystal inspection and decision making during data collection.** The first inspections relying primarily on visual appearance of the pattern are shaded in pink. If deemed satisfactory, the first images are then indexed and the mosaicity is estimated. Once the indexing succeeds, a strategy is developed based on the initial diffraction symmetry and data covering at least the asymmetric unit of the reciprocal space (plus the Friedel Bijvoet opposites in the case of anomalous data) are collected. A final risk factor is radiation damage of the crystal; it will manifest itself in diminishing diffraction over time.

h	k	l	F(hkl)	φ(hkl)
2	0	0	228.0	180.0
1	0	1	10.4	90.0
2	0	1	901.8	270.0
1	1	1	367.0	332.1
1	2	3	149.3	37.8
8	9	1	97.9	255.1
7	7	2	111.5	139.7

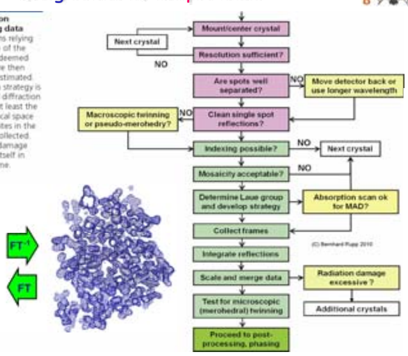

Inspection of the initial diffraction pattern: ice rings

Figure 8-25 **Ice rings.** Diffraction image (1° rotation) typical for a 3 × 3 module detector. The horizontal and vertical white lines separate the nine modules of the detector as shown in Figure 8-8, but the image is zoomed and the peripheral areas are not completely shown. When crystalline ice forms in the mother liquor or through frost deposition on the crystal, the ice crystallites are generally randomly orientated and generate concentric diffraction rings typical for a powder diffraction pattern. The lattice spacing (Å) for the ice rings is provided in the corresponding labels. The regions affected by the ice rings can be excluded from data processing with not too much detriment. Ice rings can also be used to verify the location of the primary beam position. Image and ice rings simulated using MLFSOM[13] by James Holton, UCSF.

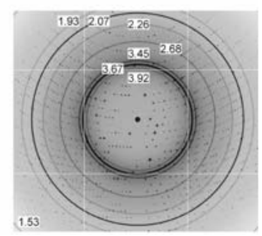

Ice rings are a powder diffraction pattern of polycrystalline ice, most of the time frost on the sample. Severe ice formation in mother liquor surrounding the crystal almost always destroys it.

Inspection of the initial diffraction pattern: exposure time

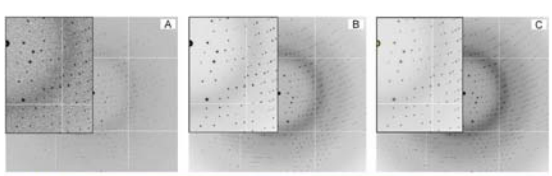

Figure 8-26 **Effects of exposure time on diffraction image quality.** The same image, exposed for successive times (30 ms, 1 s, 64 s) giving about eight times improvement in S/N between images. For each panel, the insert shows a magnification of the lower right quadrant. The first image (A) is too noisy, and we are not fully exploiting the diffraction limit of this well diffracting crystal. The second image (B) is just right; we obtain good resolution and only very few reflections are slightly saturated (yellow spot centers in insert). The third image (C) is heavily overexposed; practically all low resolution reflections are saturated (yellow spots in insert), while we are not gaining much more in terms of ultimate resolution. Images simulated using MLFSOM.[13]

Overexposure leading to detector saturation and thus loss of even a small percentage of high intensity reflections almost invariably leads to problems in phase determination – both experimental phasing and molecular replacement

Inspection of the initial diffraction pattern: reflection overlap

Figure 8-27 **Diffraction image of crystal with 300 Å unit cell.** The crystals of Rv1347c, a putative antibiotic resistance protein[11] from *M. tuberculosis*, belong to orthorhombic space group $P2_12_12_1$ with cell parameters a = 75.6 Å, b = 77.4 Å, and c = 297.6 Å, with eight molecules of 210 residues each per asymmetric unit. The data were recorded on a MAR345 image plate detector which was positioned as close as possible while still capturing all reflections up to the resolution limit of 2.2 Å. The insert shows that this is about the closest crystal–detector distance where the closely spaced reflections along **c*** are still resolved. Image files courtesy Clyde Smith and Graham Card, U. of Auckland, NZ, and SSRL, Stanford, CA.

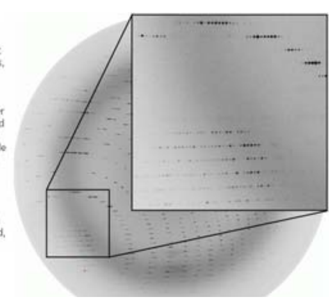

Moving the detector back or selecting longer wavelength can improve spot resolution